Molecular Imaging
Volume 16 : 1-12

DOI: 10.1177/1536012116687651
journals.sagepub.com/home/mix
SAGE

Multimodal Imaging of Patients With Gliomas Confirms ^{11}C-MET PET as a Complementary Marker to MRI for Noninvasive Tumor Grading and Intraindividual Follow-Up After Therapy

Kai R. Laukamp, MD[1,2], Florian Lindemann, PhD[3], Matthias Weckesser, MD[4], Volker Hesselmann, MD[5], Sandra Ligges, PhD[6], Johannes Wölfer, MD[7], Astrid Jeibmann, MD[8], Bastian Zinnhardt, PhD[1], Thomas Viel, PhD[1], Michael Schäfers, MD[1,4,9], Werner Paulus, MD[8,9], Walter Stummer, MD[7,9], Otmar Schober, PhD, MD[1,4,9], and Andreas H. Jacobs, MD[1,4,9,10]

Abstract

The value of combined L-(*methyl*-[^{11}C]) methionine positron-emitting tomography (MET-PET) and magnetic resonance imaging (MRI) with regard to tumor extent, entity prediction, and therapy effects in clinical routine in patients with suspicion of a brain tumor was investigated. In n = 65 patients with histologically verified brain lesions n = 70 MET-PET and MRI (T1-weighted gadolinium-enhanced [T1w-Gd] and fluid-attenuated inversion recovery or T2-weighted [FLAIR/T2w]) examinations were performed. The computer software "visualization and analysis framework volume rendering engine (Voreen)" was used for analysis of extent and intersection of tumor compartments. Binary logistic regression models were developed to differentiate between World Health Organization (WHO) tumor types/grades. Tumor sizes as defined by thresholding based on tumor-to-background ratios were significantly different as determined by MET-PET (21.6 $\pm$ 36.8 cm^3), T1w-Gd-MRI (3.9 $\pm$ 7.8 cm^3), and FLAIR/T2-MRI (64.8 $\pm$ 60.4 cm^3; $P < .001$). The MET-PET visualized tumor activity where MRI parameters were negative: PET positive tumor volume without Gd enhancement was 19.8 $\pm$ 35.0 cm^3 and without changes in FLAIR/T2 10.3 $\pm$ 25.7 cm^3. FLAIR/T2-MRI visualized greatest tumor extent with differences to MET-PET being greater in posttherapy (64.6 $\pm$ 62.7 cm^3) than in newly diagnosed patients (20.5 $\pm$ 52.6 cm^3). The binary logistic regression model differentiated between WHO tumor types (fibrillary astrocytoma II n = 10 from other gliomas n = 16) with an accuracy of 80.8% in patients at primary diagnosis. Combined PET and MRI improve the evaluation of tumor activity, extent, type/grade prediction, and therapy-induced changes in patients with glioma and serve information highly relevant for diagnosis and management.

Keywords

glioma, multimodal imaging, PET, MRI, tumor volume analysis

[1] European Institute for Molecular Imaging, Westfälische Wilhelms-Universität Münster, Munster, Germany
[2] Department of Radiology, University Hospital of Cologne, Cologne, Germany
[3] Department of Computer Science, Visualization and Computer Graphics Research Group, Westfälische Wilhelms-Universität Münster, Munster, Germany
[4] Departments of Nuclear Medicine, Westfälische Wilhelms-Universität Münster, Munster, Germany
[5] Departments of Radiology, Westfälische Wilhelms-Universität Münster, Munster, Germany
[6] Institute of Biostatistics and Clinical Research, Westfälische Wilhelms-Universität Münster, Munster, Germany
[7] Department of Neurosurgery, Westfälische Wilhelms-Universität Münster, Munster, Germany
[8] Department of Neuropathology, Westfälische Wilhelms-Universität Münster, Munster, Germany
[9] Cells-in-Motion Cluster of Excellence (EXC 1003–CiM), Westfälische Wilhelms-Universität Münster, Munster, Germany
[10] Department of Geriatric Medicine, Johanniter Hospital, Evangelische Kliniken, Bonn, Germany

Submitted: 17/05/2016. Revised: 28/11/2016. Accepted: 03/12/2016.

Corresponding Author:
Andreas H. Jacobs, European Institute for Molecular Imaging, Westfälische Wilhelms-Universität Münster, Waldeyerstraße 15, 48149 Munster, Germany.
Email: ahjacobs@uni-muenster.de

Introduction

Gliomas remain the most prevalent primary brain tumors (incidence 6-8/100.000).[1-3] Exact characterization of tumor activity, extent, type, and grade is needed for treatment. The diagnostic gold standard is open biopsy with limitations due to tumor heterogeneity.[2,4,5] The impact of imaging for patient management has increased over the past years, especially at primary diagnosis and for therapy decisions.[4,6-10]

Magnetic resonance imaging (MRI) is the method of choice at primary diagnosis and detects tumor tissue with high sensitivity at high resolution.[4] T1-weighted gadolinium-enhanced (T1w-Gd) MRI provides information about the biological activity of the tumor by detecting disruption of the blood–brain barrier (BBB).[6,7] Fluid-attenuated inversion recovery (FLAIR) and T2-weighted (T2W) MRI are assumed to depict the extent of the tumor.[1,6] However, demarcating tumor tissue from adjacent edema,[4,9,11] detection of highest malignant parts,[1,5] and differentiation among low-grade gliomas (LGG) and high-grade gliomas (HGG)[1,12] may be difficult.

Positron-emitting tomography (PET) using L-(*methyl*-[^{11}C])methionine (MET) and O-(2-[^{18}F]fluoro-ethyl)-L-tyrosine (FET) has become attractive in diagnosis of brain tumor.[4,7] The MET-PET is highly sensitive and specific in the diagnosis of brain tumors.[13] Uptake of MET is related to proliferation and neovascularization and correlates with nuclear antigen and Ki-67 expression and microvessel density.[6] The MET-PET is suited to determine most malignant tumor parts for therapy planning and ''hot spot'' definition for stereotactic biopsy[8,14-16] and to monitor treatment effects of radiotherapy and chemotherapy.[6,17,18] Furthermore, MET accumulates in LGG in the absence of disruption of the BBB.[7,19,20]

In the past, PET data in patients with brain tumors have been acquired and published in well-defined patient populations. However, there is still limited data examining the role of PET in combined use with MRI and in daily clinical routine for brain tumor patient's diagnosis and management. Therefore, assessing the usefulness of combined PET and MRI in a larger patient cohort, as it occurs in the clinical routine, is warranted.[19] The main purpose of this work was to analyze MR- and PET-based imaging results of all patients referred to the hospital with a brain tumor in a certain time frame to specify its value for clinical routine in a broad range of brain tumors with focus on gliomas. It should be pointed out that in contrast to previous reports, we ensured that for all imaging results a tumor sample is present for comparative histology. Specific features of this study are (1) to improve quantitative tumor volume (TV) analysis in an objective and reproducible manner by establishing an automated workflow within the ''visualization and analysis framework volume rendering engine'' (Voreen) software; (2) the additional analysis of the ''total tumor size (TTS)'' as the union of the TVs depicted by PET and MRI; (3) the implementation of regression models based on imaging data to predict tumor characteristics; and (4) the implementation of a visual TV depiction.

Materials and Methods

Patients

All patients with brain lesions who gave their informed consent for MET-PET from October 2009 to July 2011 (N = 185) at the Department of Nuclear Medicine, University Hospital Münster, were included in this retrospective study approved by the institutional review board (ethics committee, University Münster, approval number: 2012-307-f-N). For this type of study, the requirement to obtain informed consent was waived.

Only PET and MRI examinations (n = 70) in patients (n = 65; 4 patients obtained several imaging examinations) who received histology (biopsy and resection) within a short period of time in relation to PET and MRI (median time interval 15 days, range 1-90 days) were included. The 70 examinations were performed in 12 children and 53 adults with a median age of 48 years (range, 2-83 years). The individual patient data and indication for imaging are depicted in Supplements (I; Supplementary Tables 1 and 2; Supplementary Figure 1). Patients at primary diagnosis are referred to as ''newly diagnosed patients'' in contrast to ''posttherapy patients'' after therapy.

Histology and Grading

Diagnoses were confirmed histologically according to the World Health Organization (WHO) classification.[2] Tumor types and grades: pilocytic astrocytoma I (n = 2); vestibular schwannoma I (n = 2); neurofibroma I (n = 1); diffuse astrocytoma (n = 3); fibrillary astrocytoma II (n = 12); oligoastrocytoma II (n = 2); oligodendroglioma II (n = 1); ependymoma II (n = 2); anaplastic astrocytoma III (n = 13); anaplastic oligoastrocytoma III (n = 2); anaplastic oligodendroglioma III (n = 2); anaplastic ependymoma III (n = 1); choroid plexus carcinoma III (n = 1); glioblastoma IV (n = 19); medulloblastoma IV (n = 3); gliosarcoma IV (n = 1); cerebral b-cell lymphoma (n = 2); reactive change in brain tissue (n = 1; Supplementary Tables 1 and 2).

Imaging

The MET was synthesized according to the method of Schmitz et al.[21] Children (201.8 $\pm$ 119.0 MBq; range 39.0-382.0 MBq) and adults (348.9 $\pm$ 67.4 MBq; range 147.0-493.0 MBq) were injected with a weight-adapted MET dose. Data acquisition was performed 15 to 30 minutes postinjection of MET on an ECAT EXACT (CTI/Siemens, Erlangen, Germany; slice thickness 3.375 mm; 3D mode; iterative image reconstruction according to manufacturer's protocol).

All patients underwent a T1w-Gd MRI and a FLAIR- or T2w-MRI before or after MET-PET (median time interval 13 days). If a FLAIR-MRI was not available, a T2w-MRI was used (n = 39).

Magnetic resonance imaging of the brain was acquired using two 1.5-T scanners (Achieva 1.5-T and Intera 1.5-T; Philips, Best, the Netherlands) with identical pulse sequences and

operating interface. A 6-channel SENSE-head-coil was applied for parallel imaging. For T1w- and T2w-imaging, patients were intravenously injected with chelated gadolinium (Gadovist, Bayer Vital GmbH, Leverkusen, Germany: 1 mmol/mL, ie, 1 mL = 604.72 mg gadobutrol = 157.25 mg gadolinium) with a concentration of 0.1 mmol/kg body weight.[22] Further MRI details are indicated in Supplements (II).

Volume Analysis

The MET-PET, T1w-Gd-MR, and FLAIR/T2-MR images of the brain were analyzed and coregistered by Vinci version 3.92.[23] The Voreen was used for analysis of extent of TV and the intersection of various imaging parameters. Voreen was developed at WWU Münster (voreen.uni-muenster.de[24]) and adapted to our scientific question.[25]

The analyzed TVs were MET-PET TV (PET); T1w-Gd-MRI TV (T1); FLAIR/T2-MRI TV (FLAIR/T2); MET-PET TV without intersection with T1w-Gd-MRI TV (PwT1); MET-PET TV without intersection with FLAIR/T2-MRI TV (PwF); FLAIR/T2-MRI TV minus the MET-PET TV (FmP); and TTS as the TV based on the union of all imaging modalities.

MET-PET: The MET-PET measured TV was determined by a threshold based on the mean radioactivity concentration in the contralateral centrum semiovale plus 3 times its standard deviation. Only tissue with signals above this threshold was defined as possible tumor tissue.[26,27]

T1w-Gd-MRI And FLAIR/T2-MRI: Similar to PET, tumor tissue was defined by a threshold of the mean signal intensity in the opposite centrum semiovale plus 3 times the standard deviation. Only tissue with signals above this threshold was defined as possible tumor tissue.

To extract tissue with a physiologically high activity or signal intensity (eg, cerebellum, nasal mucosa, ventricle, and gyri), the region growing tool[28] for simple tumor structures or the random walker tool[29] for more complex tumor structures was used (details in Supplement III).[25] The TV provided by these tools were verified and if necessary adjusted simultaneously in a group of 4 experts (K.R.L., F.L., V.H., and A.H.J.). The aim of combining clearly defined thresholds with the region growing and random walker tool was to receive reliable and reproducible results and minimize intraexpert and interexpert variability in TV segmentation.[30] The tumor-to-background (T/B) radiotracer uptake ratio was calculated by dividing the maximal activity within the tumor region by the background activity in the opposite centrum semiovale.

Statistical Analysis

To differentiate between tumor types based on imaging data, a binary logistic regression model was implemented for the group of newly diagnosed patients with definitive histology (n = 26; astrocytoma I [n = 2]; astrocytoma II [n = 10]; oligoastrocytoma II [n = 1]; oligodendroglioma II [n = 1]; anaplastic astrocytoma III [n = 9]; glioblastoma IV [n = 3]). Total tumor size and T/B ratio served as covariates. Two similar models were implemented for prediction of tumor grade in newly diagnosed patients (n = 26) with TTS or T/B ratio as covariates.

Statistical analyses using IBM SPSS Statistics 20 for Windows (IBM Corporation, Somers, New York) including the implementation of the binary logistic regression models[31] were performed in cooperation with the Institute of Biostatistics and Clinical Research. Inferential statistics were intended to be exploratory (hypotheses generating) and not confirmatory. The comparison-wise type I error rate was controlled instead of the experiment-wise error rate. The significance level was set to 0.05 for 2-sided tests and 0.025 for 1-sided tests. No adjustment for multiple testing was performed. Four patients obtained several examinations that we interpreted as independent, as the date of acquisition and the stage of therapy were different. When these repeated examinations were excluded, similar results were obtained.

To enable a comprehensive TV analysis, we implemented doughnut charts to depict the relative sizes of the TV determined by the different imaging modalities.

Results

For the quantitative data analysis, we focused on glial tumor origins only (n = 60 examinations, nonglial tumors and the patient with reactive changes were not included). As gliomas are more frequent and aggressive, restricted attention to glial tumors is much more clinically relevant.

Comparison of TV as Determined By MET-PET and MRI in Patients With Gliomas

The mean TV (n = 60) was small for T1w-Gd-MRI (3.9 $\pm$ 7.8cm^3), larger for MET-PET (21.6 $\pm$ 36.8cm^3), and largest for FLAIR/T2-MRI (64.8 $\pm$ 60.4cm^3; Figure 1). The mean MET-PET TV without gadolinium enhancement (PwT1) was 19.8 $\pm$ 35.0 cm^3 and without FLAIR/T2 changes was 10.3 $\pm$ 25.7 cm^3 (Figures 1–6). These data reveal that MET-PET detects additional tumor parts that are not detected by either MRI parameter. Three examples are depicted in Figures 2 to 4. Detailed TV data are given in Supplements (IV). Individual TVs are given in supplementary Table 3. Correlations between MET-PET and WHO tumor grade as determined by histology are depicted in Supplements (V).

Tumor Volume Analysis in Patients With Gliomas After Therapy

The mean difference between FLAIR/T2-MRI TV and MET-PET TV was significantly larger in patients after therapy (64.6 $\pm$ 62.7 cm^3; n = 31) than in newly diagnosed patients (20.5 $\pm$ 52.6 cm^3; n = 29; Figure 1; 1-sided Mann-Whitney U test, P = .002). This indicates that combined FLAIR/T2-MR

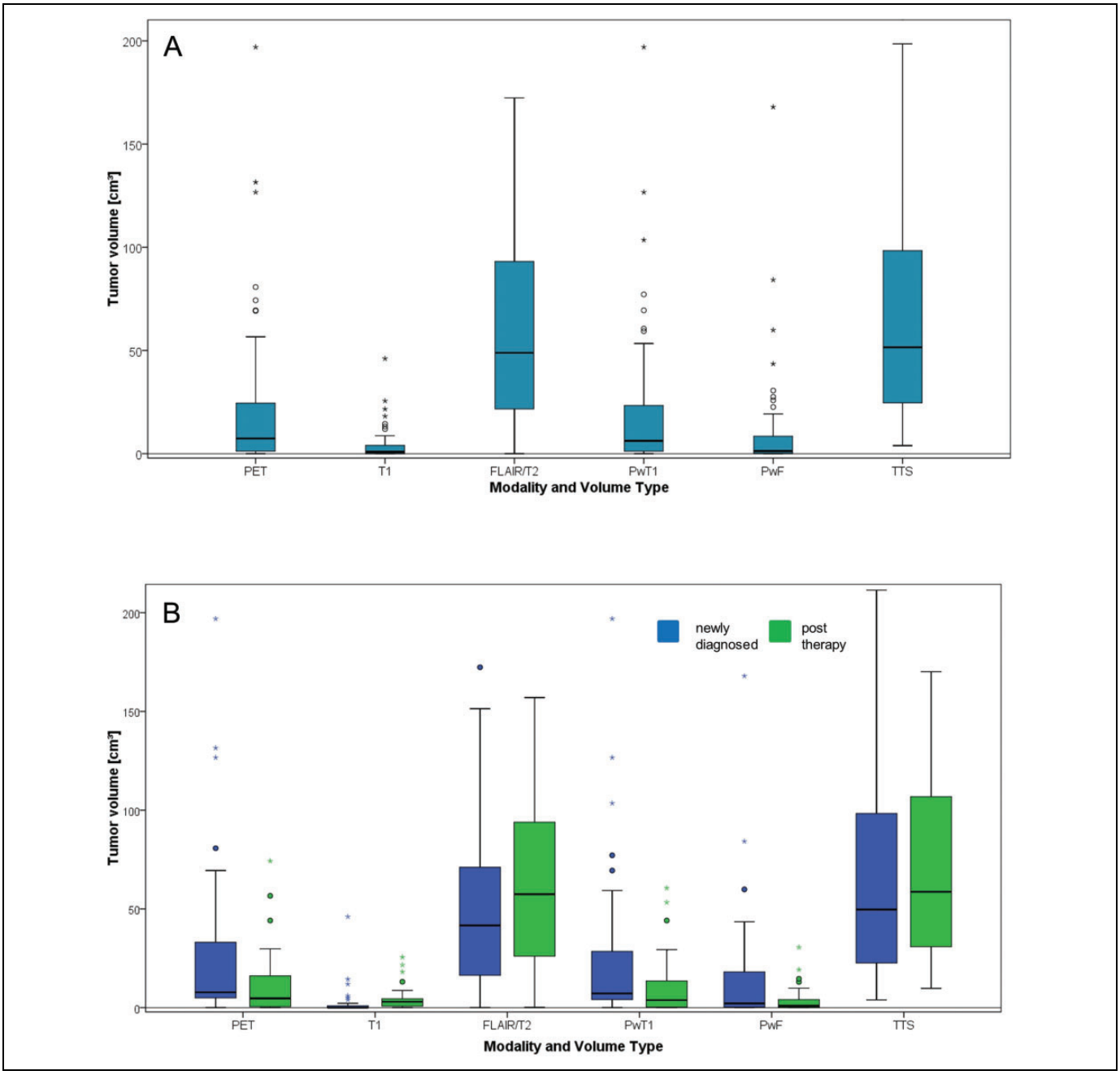

Figure 1. Parallel box plots of tumor volume (TV) as measured by visualization and analysis framework volume rendering engine (Voreen). The TV as determined by different imaging modalities for all examinations of malignant brain lesions (n = 60; A) and subgroups of newly diagnosed (n = 29) and posttherapy (n = 31) examinations (B). A, The comparison of the following TV yield significant differences (Wilcoxon signed-rank test, $P < .001$): PET versus T1; PET versus fluid-attenuated inversion recovery (FLAIR)/T2; PET versus TTS; T1 versus FLAIR/T2; T1 versus TTS; FLAIR/T2 versus TTS. B, The comparison of TV yield significant differences between newly diagnosed and posttherapy patients only for T1 (Mann-Whitney *U* test, $P < .001$) but not for PET, FLAIR/T2, PwT1, PwF, and TTS (Mann-Whitney *U* test, $P > .05$). PET = L-(*methyl*-[^{11}C]) methionine positron-emitting tomography (MET-PET); T1 = T1-weighted gadolinium-enhanced magnetic resonance imaging (T1w-Gd-MRI); FLAIR/T2 = fluid-attenuated-inversion-recovery or T2-weighted magnetic resonance imaging (FLAIR/T2-MRI); PwT1 = MET-PET TV without intersection with T1w-Gd-MRI TV; PwF = MET-PET TV without intersection with FLAIR/T2-MRI TV; TTS = total tumor size.

and MET-PET imaging differentiates therapy-induced tissue changes from metabolic active tumor tissue.

Prior studies have demonstrated the value of PET in unmasking radiation necrosis.[6,17,18] In our study, posttreatment imaging data were available for the following examinations of patients with gliomas: surgery (n = 10), surgery and radiation (n = 19), and radiation only (n = 2). Comparing volume differences in newly diagnosed and posttherapy patients who

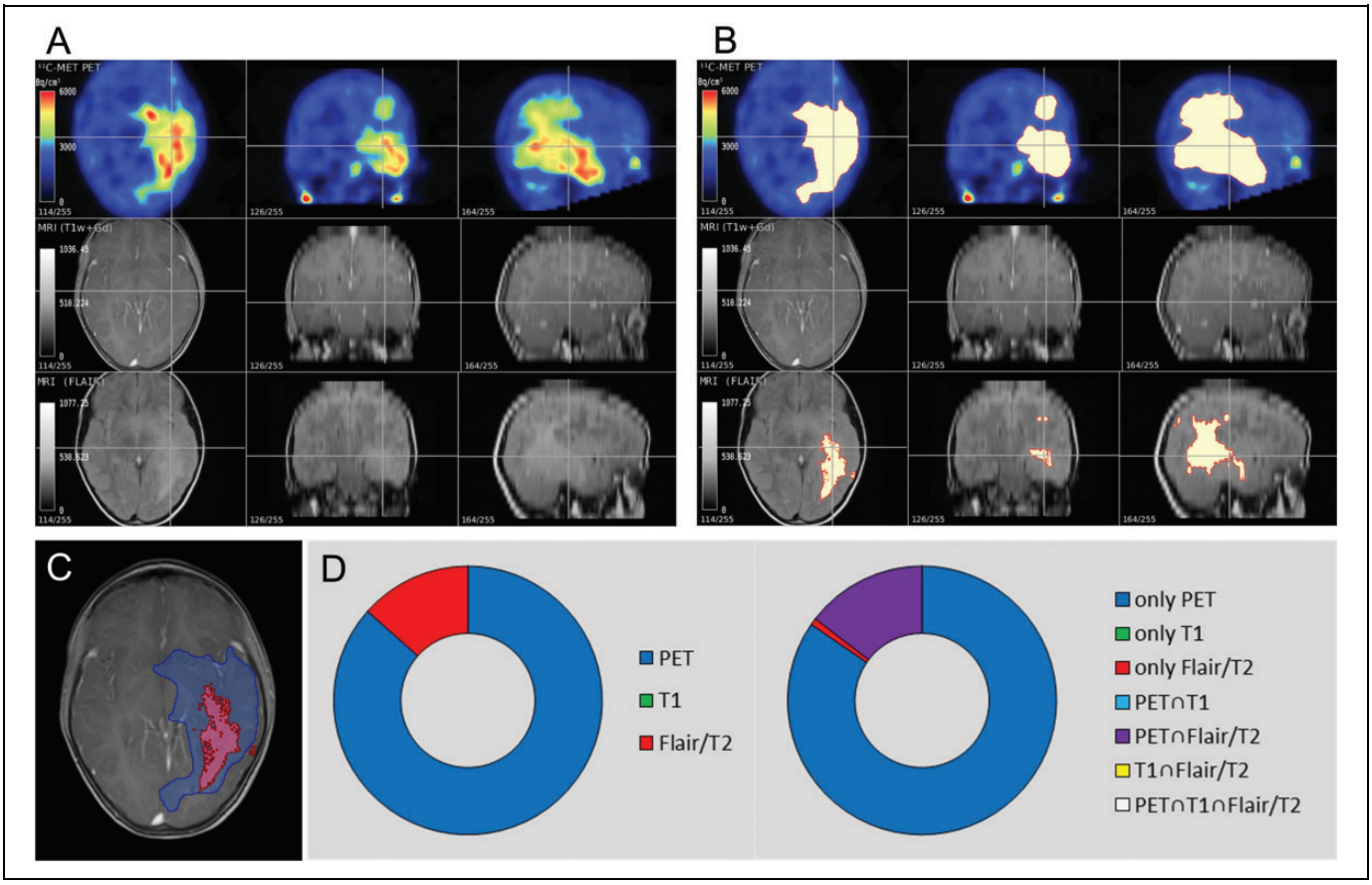

Figure 2. Positron-emitting tomography (PET) and magnetic resonance imaging (MRI) of a 9-year-old girl with newly diagnosed anaplastic astrocytoma III. L-(*methyl*-[^{11}C]) methionine (MET) accumulation in the left temporal, parietal, and occipital lobes indicates gliomatosis. The PET tumor volume (TV) is greater than the fluid-attenuated inversion recovery (FLAIR) TV (PwF TV 166cm^3). A, Unmarked images of PET, T1, and FLAIR. B, TV is marked white with red border. C, Fusion of TV shown in PET (blue) and in FLAIR (red). D, First doughnut chart: relative sizes of PET (blue), T1 (green), and FLAIR (red). Second doughnut chart shows the tumor regions where (1) only 1 modality is positive (blue [only PET positive TV], green [only T1 positive TV], and red [only FLAIR/T2 positive TV]); (2) only 2 modalities are positive (cyan [only PET∩T1], purple [only PET∩FLAIR/T2], and yellow [only T1∩FLAIR/T2]; (3) all 3 modalities are positive (white [PET∩T1∩FLAIR/T2]).

obtained only surgery, the mean difference between FLAIR/T2-MRI TV and MET-PET TV was significantly smaller (20.5 $\pm$ 52.6 cm^3) in newly diagnosed patients (n = 29, only patients with gliomas) than in patients after surgery (n = 10; 53.8 $\pm$ 37.9cm^3; 1-sided Mann-Whitney *U* test, $P = .01$).

Noninvasive Grading by Combined PET and MR Imaging

To explore the feasibility to get an indication of tumor type and grade noninvasively, we created a multinomial logistic regression model. In a first attempt, various TVs (PET, PwT1, PwF, and TTS) as well as T/B radiotracer uptake ratio were used for a combined analysis. Using these input parameters in n = 26 patients (newly diagnosed gliomas), we achieved a prediction accuracy for the WHO tumor type of >90%. The regression model needs further validation due to small patient number and the amount of covariates and different WHO tumor types.

To avoid overfitting, we further used a binary logistic regression model. This model only differentiates between 2 conditions. Thus, the low number of patients and the high amount of different WHO tumor types can be compensated. We took the tumor type that occurred most frequently (fibrillary astrocytoma II, n = 10, patient 7-16 [Supplementary Table 1]) and used the model to differentiate these from other tumor types (n = 16). The TTS showing the greatest extent of the tumor and the T/B radiotracer uptake ratio were used as covariates. This model was able to differentiate fibrillary astrocytoma II from other tumor types with an accuracy of 80.8% (model coefficient: 4.174; $P = .033$). In order to verify the quality of this model, a cross-validation was performed resulting in a classification rate of 76.9%. Only 1 patient was misclassified. This indicates the relatively high quality of the model. Integrating further covariates (imaging data) could raise the accuracy to >92%.

We also created 2 binary logistic regression models to differentiate between tumor grade (LGG vs HGG) using TTS or T/B radiotracer uptake ratio as covariates. The binary logistic regression model with the covariate TTS was able to predict the

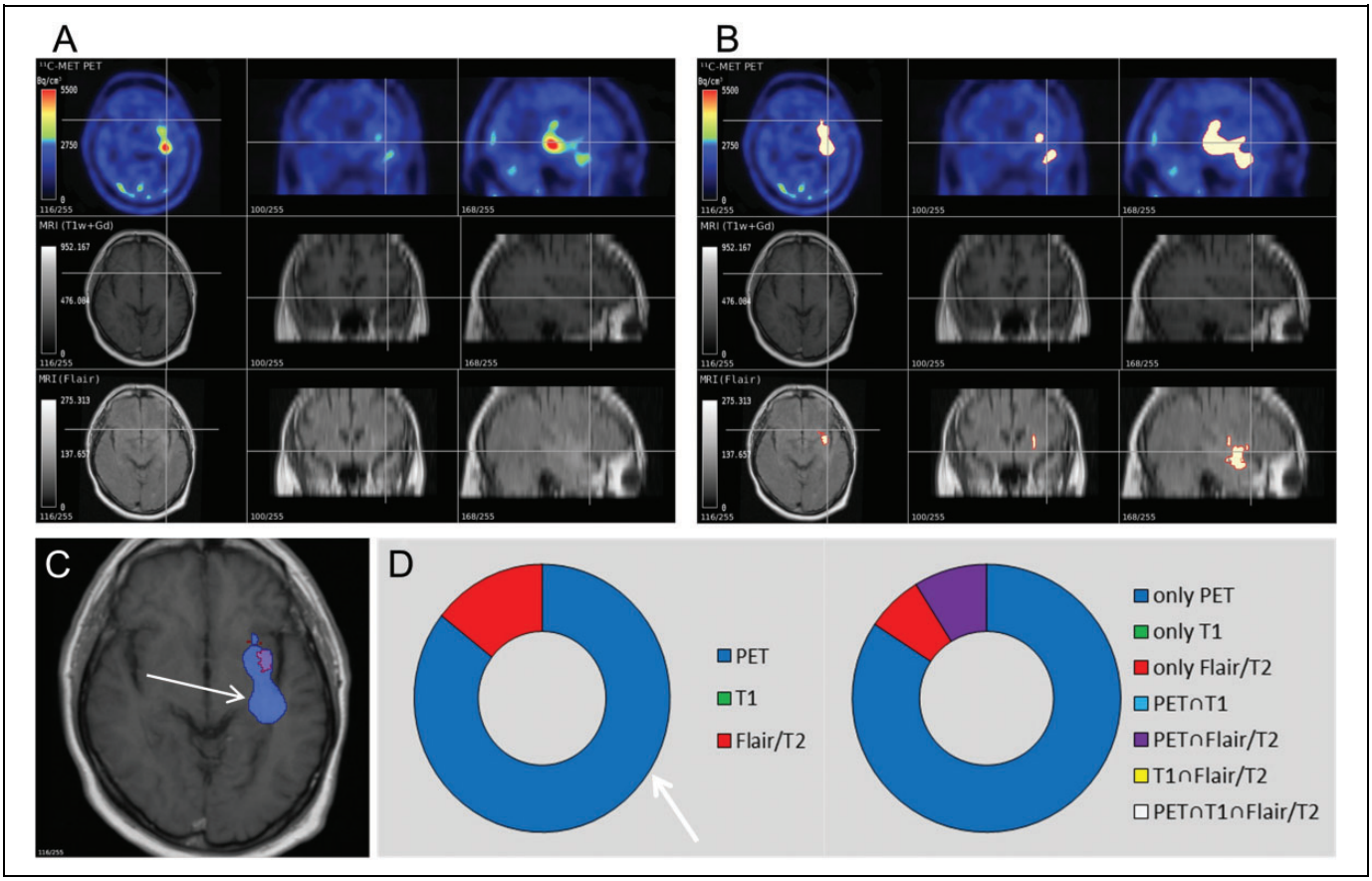

Figure 3. Positron-emitting tomography (PET) and magnetic resonance imaging (MRI) of a 62-year-old man with newly diagnosed anaplastic astrocytoma III. L-(*methyl*-[^{11}C]) methionine (MET) accumulation indicates involvement of the left temporal lobe. The PET tumor volume (TV) was larger than fluid-attenuated inversion recovery (FLAIR) TV (PwF TV 24cm^3; 2 white arrows). No gadolinium (Gd) enhancement could be detected. A, Unmarked images of PET, T1, and FLAIR. B, TV is marked white with red border. C, Fusion of TV shown in PET (blue), T1 (green), and FLAIR (red). D, Relative sizes of PET, T1 and FLAIR, and intersection TV, as explained in Figure 2.

grade of the glioma with an accuracy of 73.1% (model coefficient: 0.026; $P = .043$). The model revealed that a brain tumor with a volume above 69.2 cm^3 was more likely to be higher malignant. The binary logistic regression model with T/B radiotracer uptake value was not able to predict the malignancy of the tumor (accuracy of 61.5%; model coefficient: 0.454; $P = .272$).

Tumor Volume Analysis by Doughnut Charts

Results of the Doughnut Chart analysis are presented in Figures 2D, 3D, 4D, and 6D-F. These doughnut charts were further used for the judgment of the intraindividual follow-up after sequential therapies (Figure 5 and 6).

Intraindividual Follow-Up

Eight of 65 patients received follow-up imaging without a new biopsy. These data were not further evaluated. Four of 65 patients (vestibular schwannoma I, astrocytoma III, medulloblastoma IV, and glioblastoma) obtained more than 1 PET, MRI, and biopsy in their clinical course. In the patient with glioblastoma (No. 52, 65, and 66 in Supplementary Table 2), 3 PET and MRI examinations were performed after various treatments (Figures 5 and 6). Figures 5A and B and 6A depict the patient after resection and radiation with some remaining tumor tissue indicated by MET-PET. Tumor volume shown by MET-PET is small, whereas TV in T2w-MRI due to therapy-induced changes is large (Figure 6D). After a second resection, MET-PET reveals a new "hot spot" in the right frontal lobe adjacent to the ventricle (Figures 5C and D and 6B) partly not overlapping with T2w changes (Figure 6E), which resolved after 8 cycles of temozolomide therapy (Figure 5E and F) where no MET uptake could be delineated (Figure 6C and F). Without the additional PET information, targeted resection and chemotherapy would not have been possible in this patient.

Discussion

Our results indicate that MET-PET in clinical routine gives complementary information on tumor biology and extent to MRI. The MET-PET visualized substantial additional tumor activity in areas where both, T1w-Gd- and FLAIR/T2-MRI, were negative resulting in a greater gross TV. Differences in TV between FLAIR/T2-MRI and MET-PET were pronounced

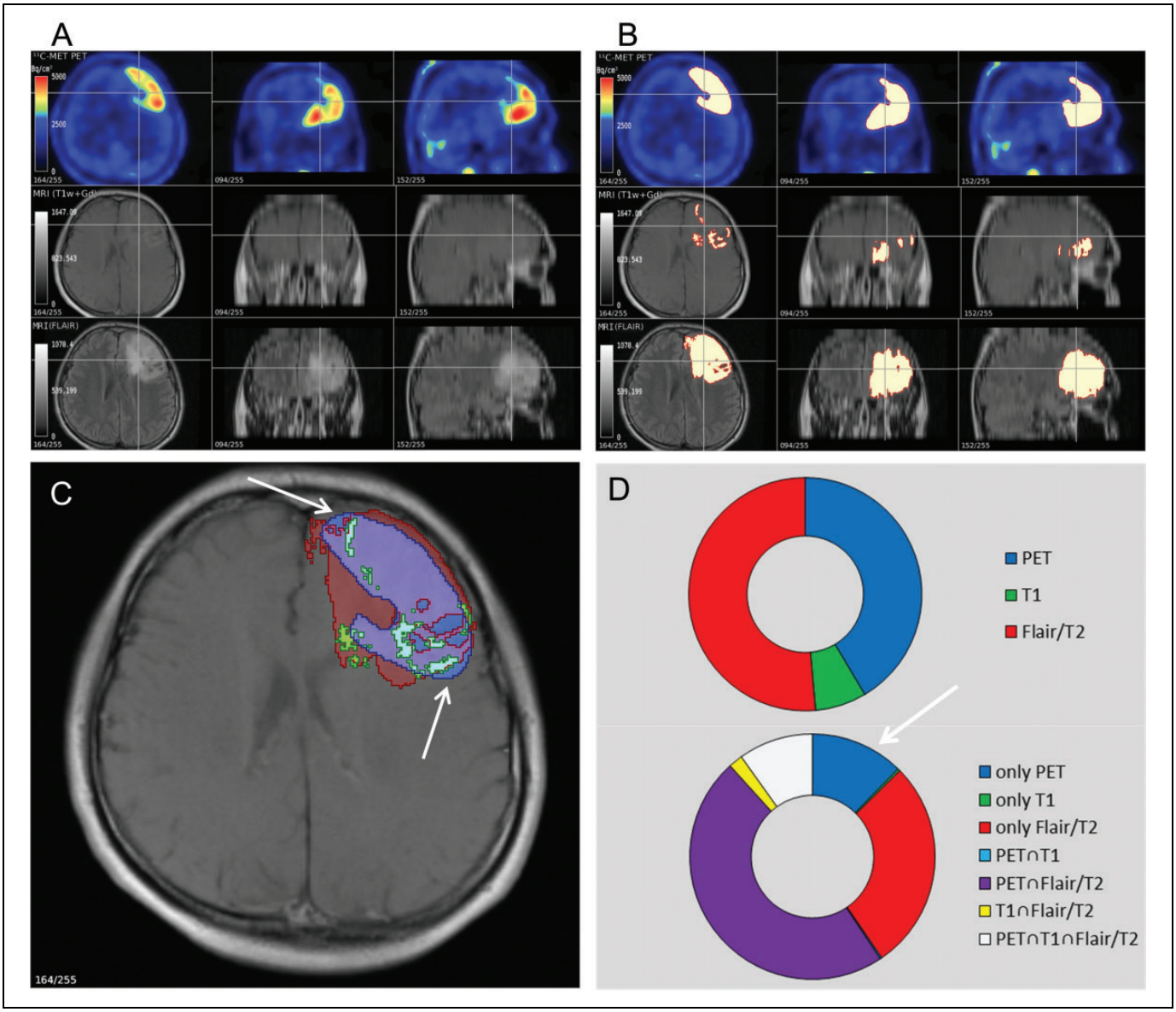

Figure 4. Positron-emitting tomography (PET) and magnetic resonance imaging (MRI) of a 36-year-old man with newly diagnosed oligoastrocytoma II. Fluid-attenuated inversion recovery (FLAIR) and PET indicate extensive glioma tissue in the left frontal lobe. T1 tumor volume (TV) was smaller. PET TV did not overlap completely with the FLAIR TV (white arrows). A, Unmarked images of PET, T1, and FLAIR. B, TV is marked white with red border. C, Fusion of TV shown in PET (blue), T1 (green) in FLAIR/T2 (red). D, Relative sizes of PET, T1 and FLAIR, and intersection TV, as explained in Figure 2.

in posttherapy patients indicating that the difference between FLAIR/T2 and MET-PET might help to delineate therapy-related tissue changes. Various imaging parameters (eg, T/B MET uptake, MET-PET TV, and TTS) showed a correlation with malignancy. The TTS showed the highest accuracy in the differentiation between low-grade (WHO tumor grades I and II) and high-grade (WHO tumor grades III and IV) tumors. The binary logistic regression model based on multimodal imaging was able to differentiate between WHO tumor types for a subgroup of patients at primary diagnosis, suggesting that noninvasive WHO tumor type determination might be possible in the future by combined PET/MR imaging.

Among the various radiotracers (^{18}F-FDG, ^{18}F-FLT, and ^{18}F-FET), we focused our investigations on ^{11}C-MET, as it is a well-established radiotracer for detection and delineation of brain tumors.[6] As has been reviewed previously[4,6-9,32] and also subjected to meta-analysis,[33,34] there is a significant number of studies (n = 37 studies at primary diagnosis with n = 1724 patients; n = 17 studies at follow-up with n = 487 patients[8]) demonstrating that MET-PET is able to differentiate between LGG and HGG with an accuracy of 60% to 70% and indicating a higher sensitivity and specificity of MET-PET in comparison to MRI for the differentiation between tumor tissue and treatment-related changes in patients with gliomas. The

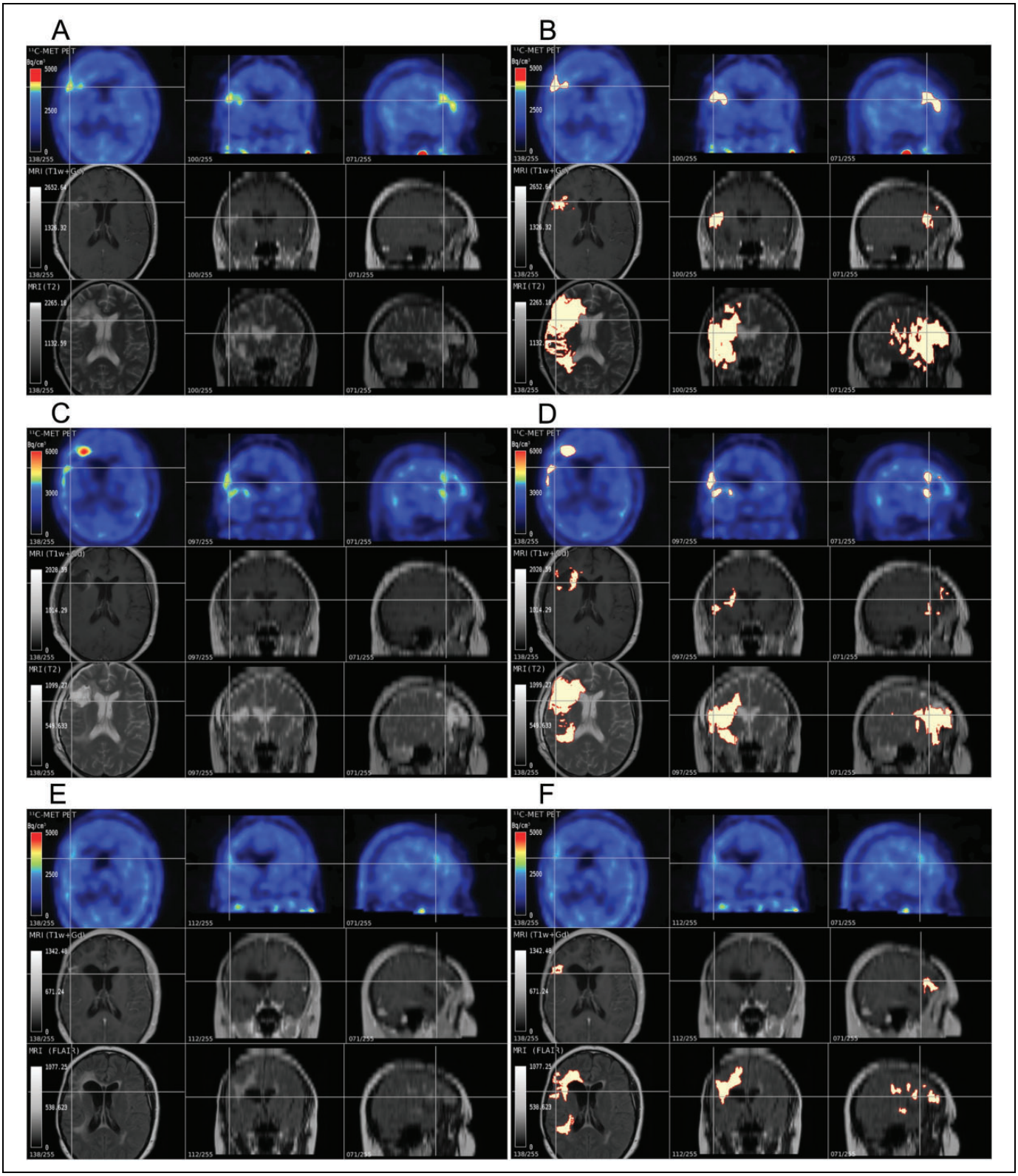

Figure 5. Imaging-guided follow-up of a 48-year-old woman with glioblastoma IV during therapy. The patient was treated by a combination of surgery, radiation, and temozolomide chemotherapy: A and B, After surgery and radiation (60 Gy) positron-emitting tomography (PET) indicates small parts of remaining active tumor tissue and T2 indicates posttherapy tissue changes. C and D, 8 months later after another surgical intervention, PET indicates more extensive active tumor tissue; therefore, chemotherapy was initiated. E and F, 7 months later after 8 cycles of temozolomide, PET and fluid-attenuated inversion recovery (FLAIR) indicate response to chemotherapy. A, C, and E, Unmarked images of PET, T1, and FLAIR/T2. B, D, and F, tumor volume (TV) is marked white with red border.

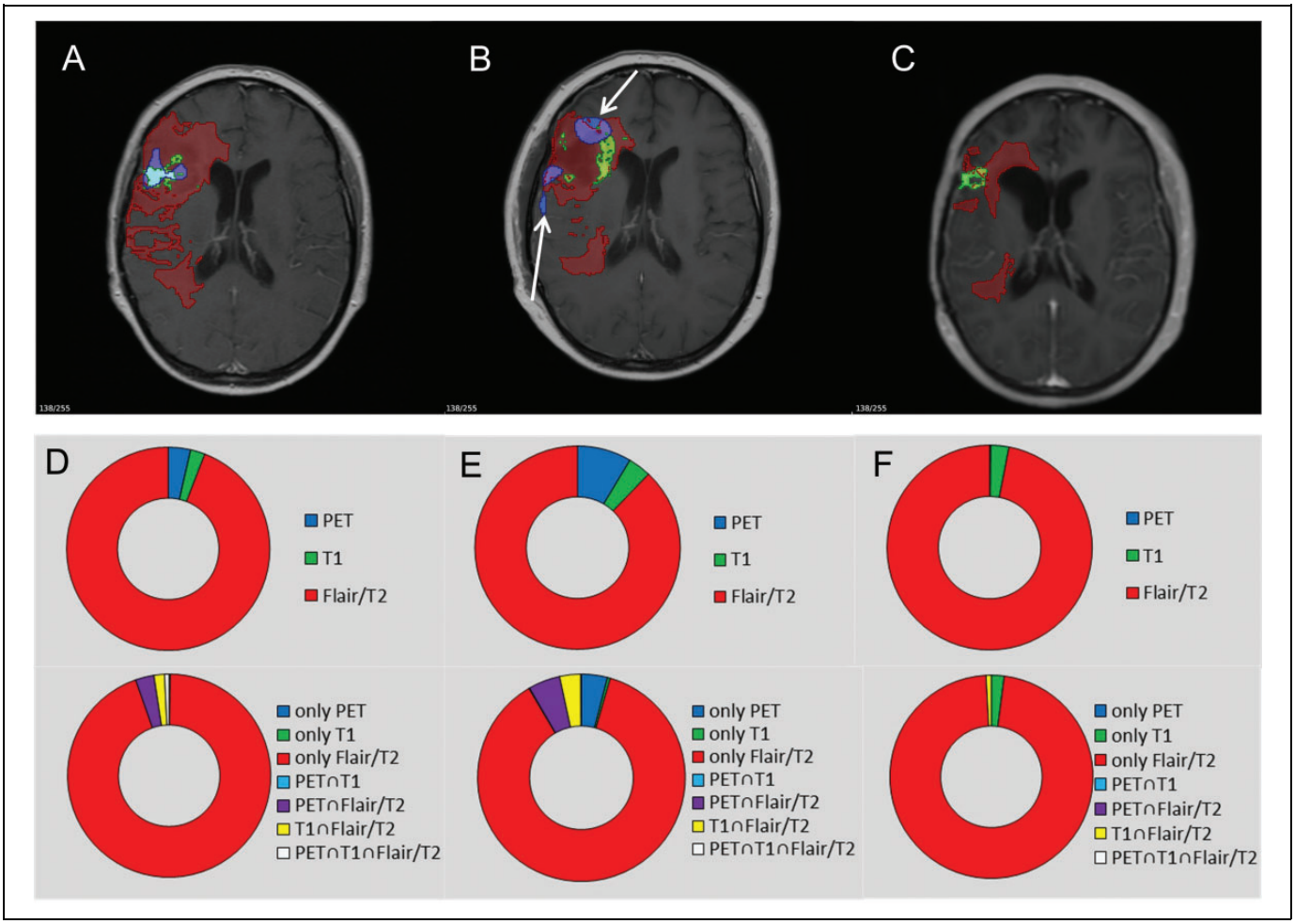

Figure 6. Volumetric analysis of 48-year-old woman with glioblastoma IV during therapy as depicted in Figure 5. A, Positron-emitting tomography (PET) indicates residual tumor activity; the volume difference to T2 is most likely due to radiation necrosis and surgery scars. B, PET shows tumor volume (TV) in areas where T2 is negative (white arrows) indicating tumor progression. C, After 8 cycles of chemotherapy PET becomes negative as indication of response to therapy. A and D, Patient after surgery and radiation (60 Gy). B and E, 8 months later after another surgical intervention. C and F, 7 months later after 8 cycles of temozolomide. A-C, Fusion of TV shown in PET (blue), T1 (green), and fluid-attenuated inversion recovery (FLAIR)/T2 (red). D-F, Relative sizes of PET, T1 and FLAIR/T2, and intersection TV, as explained in Figure 2.

MET-PET allows to detect radiotherapy and chemotherapy effects, discriminate recurrence against radiation necrosis,[6,8,17,18] and differentiate progression against stable disease.[6,8,35,36] The MET- and FET-PET give comparable diagnostic data.[37] The goal of our analysis was to demonstrate that the knowledge derived from these previous studies translates into routine clinical practice. Our analysis focused on patients who received histological grading and WHO tumor type determination within a short period of time before or after MET-PET to ensure direct correlation of imaging data and histological grading and to enable the development of the binary regression model.

Our data demonstrate that a quantitative volume analysis of brain tumors combining various imaging parameters based on PET and MRI serves important information on tumor activity and extent. The TTS improved the accuracy of prediction in the binary logistic regression model. In our subgroup of 26 patients with newly diagnosed gliomas, differentiation between LGG and HGG was predicted by the TTS (73.1%) but not by the MET T/B radiotracer uptake ratio (61.5%). It should be pointed out that with FET-PET, the kinetic analysis is being used to increase the accuracy of grading,[38] which did not work for MET-PET data.[39] The grading accuracy based on T/B ratios is influenced by oligodendroglial tumor parts, leading to higher MET or FET uptake even at low grade.[19,40] The TTS was significantly larger than MET-PET, T1w-Gd-MRI, and FLAIR/T2-MRI alone and should be taken into account for surgery and radiation planning.[8,14,16,41,42]

Exact delineation of gliomas is decisive for therapy planning. Malignant parts, missed during surgery, will lead to tumor recurrence which impacts survival.[43] Earlier studies have shown that MET-PET uptake indicates tumor infiltration which leads to recurrent tumor if missed by resection or radiation.[4,16,36,41-44] We found substantial (10.3 ± 25.7 cm^3) MET-positive tumor activity in areas where FLAIR/T2-MRI is negative.

Differentiation between recurrent tumor and radiation necrosis by MRI is not satisfactory.[4,6,7,10] Early detection of tumor recurrence with differentiation in radiation necrosis and surgery scars from active tumor tissue is important for further therapy planning.[6] The mean difference between FLAIR/T2-MRI TV and MET-PET TV was 20.5 $\pm$ 52.6 cm^3 without treatment and 64.6 $\pm$ 62.7 cm^3 after any treatment, indicating that >40 cm^3 of FLAIR/T2-MRI signal may depict tissue without any indication for biological active tumor. However, it should be noted that one of the limitations of this study is the absence of multiple stereotactic histopathological specimens of each of the abnormal imaging areas. Therefore, to determine whether high-intensity areas on T2w-/FLAIR-imaging after therapy represent active tumor or posttherapeutic changes is still difficult. In the patient group which received surgery only, the mean difference between FLAIR/T2-MRI TV and MET-PET TV was also substantial (>30 cm^3). In line with current reviews and a meta-analysis,[4,6-8,10,33] these results indicate that combined PET and MR imaging will help in the differentiation between tumor recurrence and therapy-related changes.

The gold standard for therapy decisions is histology.[35] Gliomas are heterogeneous and biopsies may miss its most malignant parts.[4,5,8,45] Multimodal imaging is able to assess this heterogeneity enabling imaging-guided stereotactic biopsy.[46] Using the TV generated by Voreen, we could create binary logistic regression models that were able to differentiate between LGG and HGG and between tumor types in a subgroup of 26 patients. Similar attempts have been used to determine tumor infiltration and WHO tumor grade.[47,48] These studies have shown that models combining several covariates might be best suited to predict tumor grade, type, or infiltration.[47-49] For the further development of this method an increased sample size is needed. Moreover, additional imaging parameters (cerebral blood volume, perfusion-/diffusion-weighted MRI, and MR spectroscopy) could be integrated.[47,48] Especially, with the implementation of combined PET/MR hybrid imaging systems simultaneous information on morphologic, metabolic, and molecular tumor parameters will serve improved diagnosis and management of patients.[4,50]

The 4 patients, in which intraindividual follow-up imaging has been performed, emphasize the value of patient-tailored, imaging-guided management with regard to improved evaluation of tumor extent and distinction between therapy-induced tissue changes and active tumor tissue. The aim to include all patients with a broad range of brain tumors may be viewed as a limitation, as it leads to a heterogeneous patient cohort. Therefore, we restricted our statistical analysis on glial tumor origins only as focused attention to glioma is more clinically relevant. However, the aim of MET-PET is to visualize biological active tumor tissue regardless of the tumor type. Our study has some limitations—It should be pointed out that in the clinical situation, a voxel-wise comparison between imaging parameters and histology is not possible for technical reasons. These limitations partly result from the aim to include the entire process of brain tumor management from diagnosis to therapy and reflect the typical patient cohort as presented in the clinical routine. It should be taken into account that especially the posttherapy imaging analysis may be confounded by tissue heterogeneity.

Conclusion

Our results indicate that MET-PET is of independent and additional value for glioma diagnosis at various disease stages in routine clinical application. Combining PET and MRI improves the delineation of the tumor extent and activity as prerequisite for appropriate surgery and radiotherapy, allows the differentiation between active tumor tissue and therapy-induced tissue changes, and, by integrating advanced volume analysis, may provide a noninvasive differentiation between WHO tumor types and grades.

Acknowledgments

The authors dedicate this manuscript specifically to our fine colleague, Delia Fahrendorf, who suddenly passed away in a tragedy in December 2015. The authors thank her for her contribution to this work. The authors thank Caecilia Spuerkel and Till Schoofs for their advice. The authors also thank Anne Kanzog for the transfer of PET and MR imaging data. The examinations were conducted in partial fulfillment of the requirements for a doctoral thesis at the University of Münster.

Declaration of Conflicting Interests

The author(s) declared no potential conflicts of interest with respect to the research, authorship, and/or publication of this article.

Funding

The author(s) disclosed receipt of the following financial support for the research, authorship, and/or publication of this article: This work was supported at least in part by BMBF grant MoBiMed (13EZ0811).

Supplemental Material

The online supplementary tables and figures are available at http://journals.sagepub.com/doi/suppl/10.1177/1536012116687651

References

1. Ullrich RT, Kracht LW, Jacobs AH. Neuroimaging in patients with gliomas. *Semin Neurol* 2008;28(4):484–494.
2. Louis DN, Ohgaki H, Wiestler OD, et al. The 2007 WHO classification of tumours of the central nervous system. *Acta Neuropathol*. 2007;114(2):97–109.
3. Sehmer EAJ, Hall GJ, Greenberg DC, et al. Incidence of glioma in a northwestern region of England, 2006-2010. *Neuro Oncol*. 2014;16(7):971–974.
4. Heiss WD, Raab P, Lanfermann H. Multimodality assessment of brain tumors and tumor recurrence. *J Nucl Med*. 2011;52(10):1585–1600.
5. Paulus W, Peiffer J. Intratumoral histologic heterogeneity of gliomas. A quantitative study. *Cancer*. 1989;64(2):442–447.
6. Dhermain FG, Hau P, Lanfermann H, Jacobs AH, van den Bent MJ. Advanced MRI and PET imaging for assessment of treatment response in patients with gliomas. *Lancet Neurol*. 2010;9(9):906–920.

7. Galldiks N, Langen KJ, Pope WB. From the clinician's point of view—What is the status quo of positron emission tomography in patients with brain tumors? *Neuro Oncol*. 2015;17(11): 1434–1444.
8. Glaudemans AWJM, Enting RH, Heesters MAAM, et al. Value of 11C-methionine PET in imaging brain tumours and metastases. *Eur J Nucl Med Mol Imaging*. 2013;40(4):615–635.
9. Fink JR, Muzi M, Peck M, Krohn KA. Multimodality brain tumor imaging: MR imaging, PET, and PET/MR imaging. *J Nucl Med*. 2015;56(10):1554–1561.
10. Jacobs AH, Kracht LW, Gossmann A, et al. Imaging in neurooncology. *NeuroRx*. 2005;2(2):333–347.
11. Artzi M, Bokstein F, Blumenthal DT, et al. Differentiation between vasogenic-edema versus tumor-infiltrative area in patients with glioblastoma during bevacizumab therapy: a longitudinal MRI study. *Eur J Radiol*. 2014;83(7):1250–1256.
12. Scott JN, Brasher PMA, Sevick RJ, Rewcastle NB, Forsyth PA. How often are nonenhancing supratentorial gliomas malignant? A population study. *Neurology*. 2002;59(6):947–949.
13. Dunet V, Pomoni A, Hottinger A, Nicod-Lalonde M, Prior JO. Performance of 18F-FET versus 18F-FDG-PET for the diagnosis and grading of brain tumors: systematic review and meta-analysis. *Neuro Oncol*. 2015;18(3):426–434.
14. Pirotte B, Goldman S, Dewitte O, et al. Integrated positron emission tomography and magnetic resonance imaging-guided resection of brain tumors: a report of 103 consecutive procedures. *J Neurosurg*. 2006;104(2):238–253.
15. Pirotte B, Goldman S, Massager N, et al. Comparison of 18F-FDG and 11C-methionine for PET-guided stereotactic brain biopsy of gliomas. *J Nucl Med*. 2004;45(8):1293–1298.
16. Lee IH, Piert M, Gomez-Hassan D, et al. Association of 11C-methionine PET uptake with site of failure after concurrent temozolomide and radiation for primary glioblastoma multiforme. *Int J Radiat Oncol Biol Phys*. 2009;73(2):479–485.
17. Terakawa Y, Tsuyuguchi N, Iwai Y, et al. Diagnostic accuracy of 11C-methionine PET for differentiation of recurrent brain tumors from radiation necrosis after radiotherapy. *J Nucl Med*. 2008; 49(5):694–699.
18. Piroth MD, Pinkawa M, Holy R, et al. Prognostic value of early [18F]fluoroethyltyrosine positron emission tomography after radiochemotherapy in glioblastoma multiforme. *Int J Radiat Oncol Biol Phys*. 2011;80(1):176–184.
19. Hutterer M, Nowosielski M, Putzer D, et al. [18F]-fluoro-ethyl-L-tyrosine PET: a valuable diagnostic tool in neuro-oncology, but not all that glitters is glioma. *Neuro Oncol*. 2013;15(3):341–351.
20. Rapp M, Floeth FW, Felsberg J, et al. Clinical value of O-(2-[(18)F]-fluoroethyl)-L-tyrosine positron emission tomography in patients with low-grade glioma. *Neurosurg Focus*. 2013;34(2):E3.
21. Schmitz F, Plenevaux A, Del-Fiore G, Lemaire C, Comar D, Luxen A. Fast routine production of l-[11C-methyl]methionine with Al2O3KF. *Appl Radiat Isot*. 1995;46(9):893–897.
22. Fahrendorf D, Schwindt W, Wölfer J, et al. Benefits of contrast-enhanced SWI in patients with glioblastoma multiforme. *Eur Radiol*. 2013;23(10):2868–2879.
23. Vollmar S, Sue M, Klein J, Jacobs A, Herholz K. VINCI: Volume imaging in neurological research, co-registration and ROIs included. In: Kremer K, Macho V, eds. *Res Sci Comput 2003 Göttingen, Ger Gesellschaft für wissenschaftliche Datenverarbeitung*; 2004:115–131.
24. Meyer-Spradow J, Ropinski T, Mensmann J, Hinrichs K. Voreen: a rapid-prototyping environment for ray-casting-based volume visualizations. *IEEE Comput Graph Appl*. 2009;29(6):6–13.
25. Lindemann F, Laukamp KR, Jacobs A, Hinrichs K. Interactive Comparative Visualization of Multimodal Brain Tumor Segmentation Data. *Eurographics - Vision, Modeling, and Visualization*; 2013:105–112. http://dx.doi.org/10.2312/PE.VMV.VMV13.105-112. Eurographics – European Association for Computer Graphics.
26. Weckesser M, Langen KJ, Rickert CH, et al. O-(2-[18F]fluoroethyl)-L-tyrosine PET in the clinical evaluation of primary brain tumours. *Eur J Nucl Med Mol Imaging*. 2005;32(4):422–429.
27. Weckesser M, Griessmeier M, Schmidt D, et al. Iodine-123 alpha-methyl tyrosine single-photon emission tomography of cerebral gliomas: standardised evaluation of tumour uptake and extent. *Eur J Nucl Med*. 1998;25(2):150–156.
28. Adams R, Bischof L. Seeded Region Growing. *IEEE Trans Pattern Anal Mach Intell*. 1994;16(6):641–647.
29. Prassni JS, Ropinski T, Hinrichs K. Uncertainty-aware guided volume segmentation. *IEEE Trans Vis Comput Graph*. 2010; 16(6):1358–1365.
30. Warfield SK, Zou KH, Wells WM. Simultaneous truth and performance level estimation (STAPLE): an algorithm for the validation of image segmentation. *IEEE Trans Med Imaging*. 2004; 23(7):903–921.
31. R Core Team. *R: A Language and Environment for Statistical Computing*. Austria: R Found Stat Comput Vienna; 2013.
32. la Fougère C, Suchorska B, Bartenstein P, Kreth FW, Tonn JC. Molecular imaging of gliomas with PET: opportunities and limitations. *Neuro Oncol*. 2011;13(8):806–819.
33. Nihashi T, Dahabreh IJ, Terasawa T. Diagnostic accuracy of PET for recurrent glioma diagnosis: a meta-analysis. *AJNR Am J Neuroradiol*. 2013;34(5):944–950.
34. Deng SM, Zhang B, Wu YW, Zhang W, Chen YY. Detection of glioma recurrence by ^{11}C-methionine positron emission tomography and dynamic susceptibility contrast-enhanced magnetic resonance imaging: a meta-analysis. *Nucl Med Commun*. 2013;34(8): 758–766.
35. Ullrich RT, Kracht L, Brunn A, et al. Methyl-L-11C-methionine PET as a diagnostic marker for malignant progression in patients with glioma. *J Nucl Med*. 2009;50(12):1962–1968.
36. Galldiks N, Ullrich R, Schroeter M, Fink GR, Jacobs AH, Kracht LW. Volumetry of [(11)C]-methionine PET uptake and MRI contrast enhancement in patients with recurrent glioblastoma multiforme. *Eur J Nucl Med Mol Imaging*. 2010;37(1):84–92.
37. Grosu AL, Astner ST, Riedel E, et al. An interindividual comparison of O-(2-[18F]fluoroethyl)-L-tyrosine (FET)- and L-[methyl-11C]methionine (MET)-PET in patients with brain gliomas and metastases. *Int J Radiat Oncol Biol Phys*. 2011; 81(4):1049–1058.
38. Galldiks N, Stoffels G, Ruge MI, et al. Role of O-(2-18F-fluoroethyl)-L-tyrosine PET as a diagnostic tool for detection of

malignant progression in patients with low-grade glioma. *J Nucl Med*. 2013;54(12):2046–2054.
39. Moulin-Romsée G, D'Hondt E, de Groot T, et al. Non-invasive grading of brain tumours using dynamic amino acid PET imaging: does it work for 11C-methionine? *Eur J Nucl Med Mol Imaging*. 2007;34(12):2082–2087.
40. Hatakeyama T, Kawai N, Nishiyama Y, et al. 11C-methionine (MET) and 18F-fluorothymidine (FLT) PET in patients with newly diagnosed glioma. *Eur J Nucl Med Mol Imaging*. 2008; 35(11):2009–2017.
41. Tanaka Y, Nariai T, Momose T, et al. Glioma surgery using a multimodal navigation system with integrated metabolic images. *J Neurosurg*. 2009;110(1):163–172.
42. Rieken S, Habermehl D, Giesel FL, et al. Analysis of FET-PET imaging for target volume definition in patients with gliomas treated with conformal radiotherapy. *Radiother Oncol*. 2013;109(3):487–492.
43. Pirotte BJM, Levivier M, Goldman S, et al. Positron emission tomography-guided volumetric resection of supratentorial high-grade gliomas: a survival analysis in 66 consecutive patients. *Neurosurgery*. 2009;64(3):471–481.
44. Kracht LW, Miletic H, Busch S, et al. Delineation of brain tumor extent with [11C]L-methionine positron emission tomography: local comparison with stereotactic histopathology. *Clin Cancer Res*. 2004;10(21):7163–7170.
45. Jackson RJ, Fuller GN, Abi-Said D, et al. Limitations of stereotactic biopsy in the initial management of gliomas. *Neuro Oncol*. 2001;3(3):193–200.
46. Gempt J, Soehngen E, Förster S, et al. Multimodal imaging in cerebral gliomas and its neuropathological correlation. *Eur J Radiol*. 2014;83(5):829–834.
47. Roy B, Gupta RK, Maudsley AA, et al. Utility of multiparametric 3-T MRI for glioma characterization. *Neuroradiology*. 2013; 55(5):603–613.
48. Durst CR, Raghavan P, Shaffrey ME, et al. Multimodal MR imaging model to predict tumor infiltration in patients with gliomas. *Neuroradiology*. 2014;56(2):107–115.
49. Law M, Young R, Babb J, et al. Comparing perfusion metrics obtained from a single compartment versus pharmacokinetic modeling methods using dynamic susceptibility contrast-enhanced perfusion MR imaging with glioma grade. *AJNR Am J Neuroradiol*. 2006;27(9):1975–1982.
50. Boss A, Bisdas S, Kolb A, et al. Hybrid PET/MRI of intracranial masses: initial experiences and comparison to PET/CT. *J Nucl Med*. 2010;51(8):1198–1205.